Programmable Analogic Cellular Optical Computer using Bacteriorhodopsin as Analog Rewriteable Image Memory

Szabolcs TŐKÉS[1], László.ORZÓ[1], György VÁRÓ[2], András DÉR[2], Pál ORMOS[2] and Tamás ROSKA[1]

[1]*Analogical and Neural Computing Research Laboratory, Computer and Automation Institute, H-1111 Budapest, Hungary*
[2]*SZBK Szeged, Hungary*

ABSTRACT. Bacteriorhodopsin has been proved to be an outstanding candidate for reversible, transient, real-time, holographic material. Here we show our preliminary experimental investigation of its applicability as a transient analog memory, concentrating on its possible utilization in optical CNN implementations and in programmable opto-electronic analogic CNN computers (POAC). Different possible architectures and the technical details of its applicability are also discussed. The main objective is to provide a framework for the implementation of Programmable Opto-Electronic Analogic CNN Computers embedding CNN Universal Chips. Specifically, a new method for optical CNN implementation is provided and some details are experimentally studied. The POAC architecture includes the integration of an optical processing system, such as a joint transform correlator using bacteriorhodopsin as holographic material, with the fast spatio-temporal processing capabilities of a CNN-UM chip. We have built and tested an optical sub-unit of this experimental opto-electronic architecture to examine their processing capabilities in complex target recognition tasks. The main idea is to introduce stored programmability into optical computing. The specification of the necessary holographic material for POAC application is given. Some measurement results on BR samples are presented.

1 Introduction

In this report we try to summarize the known physical and chemical properties of Bacteriorhodopsin (BR) [1] and some different modified BR forms [2], [3],[4], [5] from the point of view of its possible utilization as a transient holographic recording material, especially as a part of the POAC system [6].

Our goal is to define the possible architectures for the efficient application of this material within this framework. Based on the known properties of different modified and molecular-engineered forms of BR we can estimate its potential speed and capacity within a POAC device using it as a dynamic holographic material. Feasibility of the different possible architectures is discussed. First we summarize the basic properties of BR. Later we describe the fundamental structure and properties of the CNN paradigm [7], [8] [9], [10], which optical implementation and application is aimed. Next we outline the scope of the POAC system within we intend to use BR as a rewriteable holographic memory and dynamic holographic material. At last we describe some of the prospective architectures and some results of our preliminary measurements, which tries to define the applicability of BR and its modified forms.

2 Bacteriorhodopsin

2.1 History & Biological primers

BR is a stable transmembrane protein of an archea bacterium, Halobacterium (Halobacterium Halobium). This bacterium lives in salt marshes. Halobacterium can survive even in bizarre environmental conditions. It prefers extremely high sodium chloride concentrations [1],[2].

BR, itself, is a photon-driven proton pump. Halobacteriums use this protein to utilize the energy of light, when dissolved oxygen concentration drop below the levels sufficient to sustain respirative oxidative phosphorylation. After the absorption of a photon BR pumps one proton out of the cell through the cell membrane. Arising proton gradient provides the energy for the cell. This type of energy is later transformed to chemical form of energy - ATP molecules - by the application of ATP synthase enzymes.

2.2 Physical and Chemical properties

BR molecules consist of seven α-helical sub-domains. These parts of the protein form a hole, which is occupied by a co-factor, the retinal molecule. The structure of the BR molecule is intensively studied and relatively well known. BR molecules aggregate uni-axially oriented, hexagonal, trimer structure. This hexagonal, crystal-like structure assembles into large clustered patches on the membrane.

2.3 Photocycle

After the absorption of a photon BR goes through a sequence of chemical and physical changes [1], [11], [12]. It is including the retinal molecule's all-trans – 13-cis transformation, shifts of charges within the protein, movement of protons, that is protonation, deprotonation, and several conformational changes as well. The above characteristic changes are reflected - and manifested primarily - in the changes of the BR's absorption spectrum. Different states have different lifetimes and characteristic absorption spectra. After the photon absorption and proton transfer, BR sooner or later recovers to its initial conformation. The whole sequence of transitions is called the photocycle of the BR. The quantum yield of the photocycle is relatively high (0.67). The above mentioned characteristic changes in the absorption spectra can be used for analog memory storage. The main steps of the BR photocycle absorption spectra are depicted on the next figure. The characteristic life times of the different states is described in the succeeding table:

	500fs	10ps	2μs	40 μs	7ms	4ms
BR_{570}	$\rightarrow J_{625}$	$\rightarrow K_{600}$	$\leftrightarrow L_{550}$	$\leftrightarrow M_{412}$	$\leftrightarrow N_{520}$	$\leftrightarrow O_{640} \leftrightarrow BR_{570}$

Table 1. Characteristic times of the BR photocycle states.

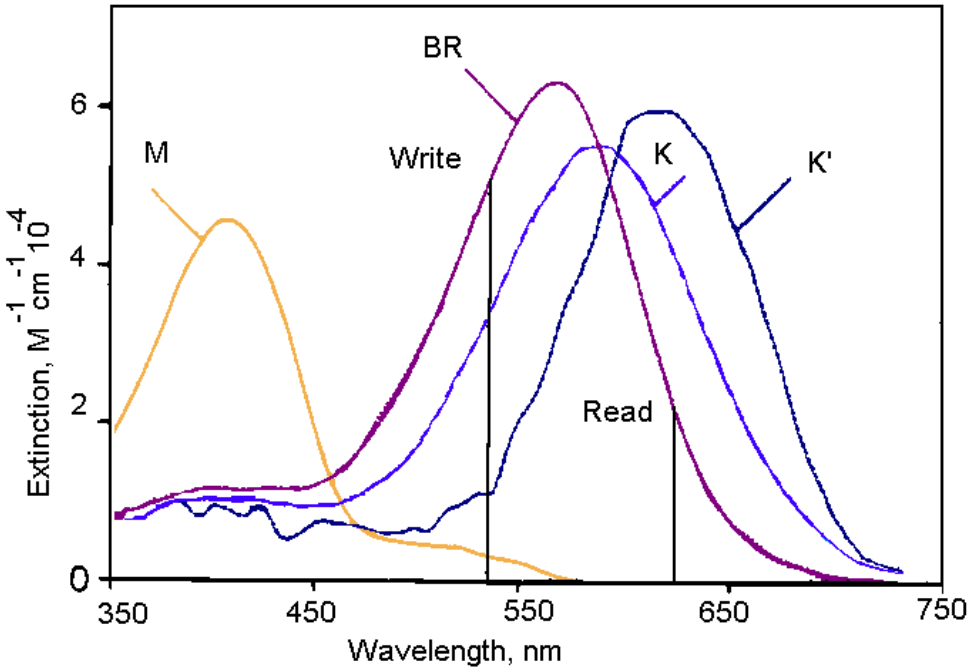

Figure 1. BR's absorption spectra at different states of the photocycle. Their difference can be used for identification and so to write and read data in this material.

Being aware of the BR's structure and its detailed molecular dynamics, even molecular engineered alteration of it is possible. Different biologically, chemically and physically modified BR forms are available [13], [14], [15]. Several different types of utilization of BR have been suggested. An overview of these applications can be found in the paper of Birge [16], [17], [18], [19], [15], [20], [21], [23] (These includes random access thin film memories, neural-type logic gates, photon counters and photovoltaic converters, reversible holographic media, artificial retinas picosecond photodetectors, spatial light modulators, associative memories, two-photon volumetric memories, holographic correlators, nonlinear optical filters, dynamic time-average interferometers, optical limiters, pattern recognition systems, multilevel logic gates, optical computing, and branched-photocycle volumetric memories.) In this paper the BR's applicability as a transient holographic recording material is examined particularly.

2.4 BR as a transient holographic material - Speed & resolution

It is usually claimed [1], [15] that the BR has extremely high spatial resolution: higher than 5000 lines/mm. This resolution even exceeds the commonly applied optical system's capabilities. This high spatial resolution assures the feasibility of dual axis JTC implementation (see later). Sensitivity of the material is relatively low (1-80 mJ/cm^2) [vsedolodov, hampp], but it is even better than those holographic materials, which have comparable resolution [osterhelt] and does not require further evaluation. The writing speed of BR can be remarkably high, but of course, it depends on which states or state transitions of the photocycle are used. Usually the BR's initial state (bR) and another relatively stable intermedier (M) states are used. The bR to M transformation takes about 40μsec. This speed seems to be satisfactory for our transient holographic recording purposes, but using other states and different modified forms of BR even much higher speed can be achieved [25], [26], [27] (e.g. bR-K transition takes only about 500 fsec)(see later). One of the main problems with the utilization of BR as a temporary holographic material, is the relatively long recovery time of the photocycle (M to bR transition can take several hundreds of milliseconds and even second if we use different kinds of

modified BR samples). If we use fresh material after all write-read cycle we can solve this problem. It can be accomplished by the appropriate replacement, shift of the recording material. There is another, technically more convenient way to overcome this restriction: Intensive blue light drives back the BR's M state to bR state within 50-100μsec [28]. Non-coherent intense blue light is relatively easy to produce.

So BR seems to be an adequate dynamic holographic recording medium [29], even at a very high speed. BR can be read and write more than one million times without considerable degradation. It is stable for months or years and persists in harsh environmental conditions. It is resistant for heat and irradiation. It is protected against oxygen and stable in a really wide range of pH (from pH 1 to 10).

3 The CNN frame of computation

The CNN frame of computation [7], [8] can be characterized by a coupled dynamical system of identical first order cells located at the node points of an *MxN* grid and described by the following equations (standard continuous-time CNN):

$$\begin{aligned} C\frac{d}{dt}x_{ij}(t) &= -R^{-1}x_{ij}(t) + \sum_{kl\in S_r} A_{ij,kl}\,y_{kl}(t) + \sum_{kl\in S_r} B_{ij,kl}\,u_{kl}(t) + z \\ &= -R^{-1}x_{ij}(t) + \sum_{kl\in S_r} A_{ij,kl}\,y_{kl}(t) + z_{ij} \\ y_{ij}(t) &= f(x_{ij}(t)) = 0.5\,(|x_{ij}(t)+1| - |x_{ij}(t)-1|) \end{aligned} \qquad (1)$$

where :

$$-1 \le x_{ij}(0) \le 1,\ -1 \le u_{ij}(t) \le 1\ ,\qquad |z| \le z_{\max}$$

$$1 \le i \le M,\ 1 \le j \le N$$

(The extremal values come from the nonlinearity and sometimes are not specified: u; x, z… especially x can be bigger than 1 in the CNN-UM and only the special implementation limitates their value) where u_{ij}, x_{ij}, y_{ij} are the input, state and output voltage of the specified CNN cell, respectively. The subscript *ij* refers to a grid point associated with a cell on the 2D grid, and $kl \in S_r$ is a grid point in the neighborhood within the radius *r* of the cell *ij* (S_r is referred to as the sphere of influence). $A_{ij,kl}$ represents the linear feedback, $B_{ij,kl}$ the linear control, while *z* is the bias (cell current). The output characteristic *f* is a sigmoid-like piecewise-linear function. The time constant of a CNN cell is determined by the linear capacitor (*C*) and the linear resistor (*R*) and it can be expressed as $\tau = RC$. Without loss of generality $R = 1$ and $C = 1$ can be considered. The boundary condition is assumed to be constant or reflected type.

3.1 The CNN Universal Machine and Chip Implementations

The CNN Universal Machine (CNN-UM), is a stored program nonlinear array computer [9], [10]. This new architecture is able to combine analog array operations with local logic efficiently. To ensure programmability, a global programming unit was added to the array, and to make possible an efficient use and reuse of intermediate results, each computing cell was extended by local memories. In addition to local storage, every cell is equipped with local sensors and additional circuitry to perform cell-wise analog and logical operations. The architecture of the CNN-UM is shown in **Figure 2**.

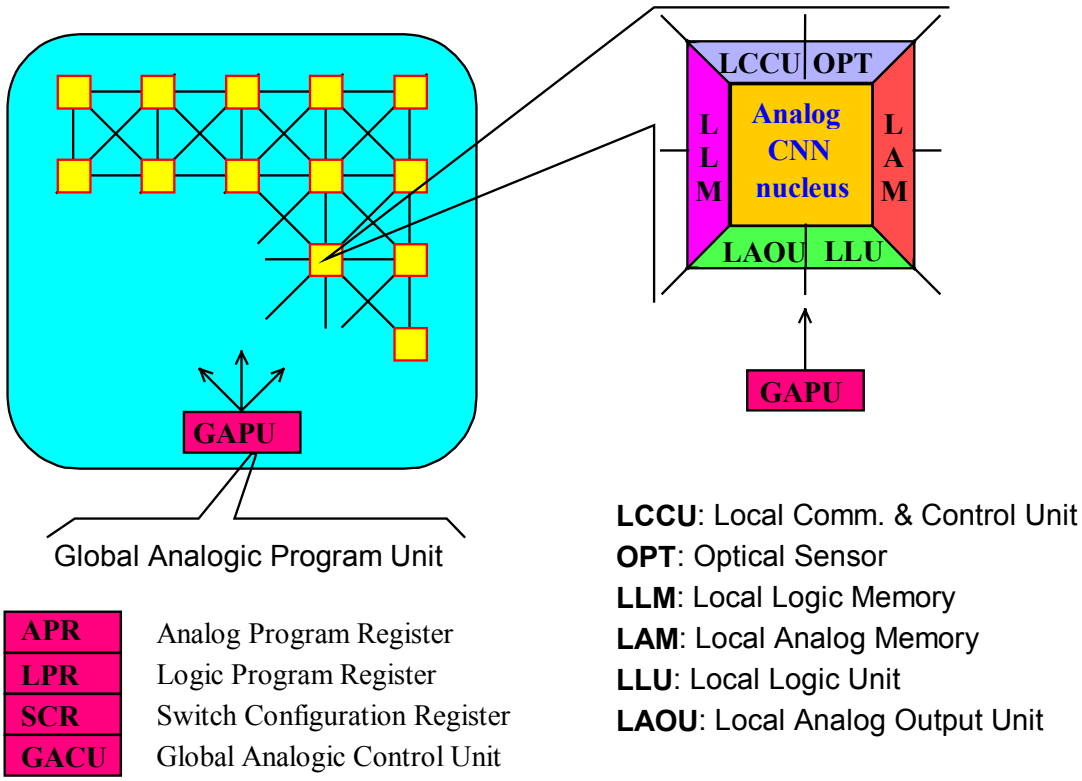

Figure 2. The architecture of the CNN Universal Machine, the analogic array supercomputer.

As illustrated in Figure 2 the CNN-UM is built around the dynamic computing core of a simple CNN. The input (image) can be acquired through the sensory array (e.g. OPT: Optical Sensor). Local memories store analog (LAM: Local Analog Memory) and logic (LLM: Local Logical Memory) values in each cell. A Local Analog Output Unit (LAOU) and a Local Logic Unit (LLU) perform cell-wise analog and logic operations on the stored values. The output is always transferred to one of the local memories. The Local Communication and Control Unit (LCCU) provides for communication between the extended cells and the central programming unit of the machine, the Global Analogic Programming Unit (GAPU). The GAPU has four functional blocks. The Analog Program Register (APR) stores the analog program instructions, the CNN templates. In case of linear templates, for a connectivity $r = 1$ a set of 19 real numbers have to be stored (this is even less for both linear and nonlinear templates assuming spatial symmetry). All other units within the GAPU are logic registers containing the control codes for handling the cell array. The Local Program Register (LPR) contains control sequences for the individual cell's LLU, the Switch Configuration Register (SCR) stores the codes to initiate the different switch configurations when accessing the different functional units (e.g. whether to run a linear or nonlinear template). The Global Analogic Control Unit (GACU) stores the instruction sequence of the main (analogic) program. The GACU also controls the timing, sequence of instructions and data transfers on the chip and synchronizes the communication with any external controlling device.

Synthesizing an analogic algorithm running on the CNN-UM the designer should decompose the solution in a sequence of analog and logical operations. A limited number of intermediate results can be locally stored and combined. Some of these outputs can be used as a bias map (space variant current) or fixed-state map (space-variant mask) in the next operation providing spatial adaptivity to the algorithms without introducing more refined cell couplings. Both the linear and the nonlinear templates define analog operations. The output can be defined either fixed or non-fixed state of the network (equilibrium and non-equilibrium computing) depending on the nature of an operation and control of the transient length. Elementary logical (**NOT**, **AND**, **OR,** *etc.*) and arithmetical (**ADD**, **SUB**) operations are implemented and can be used on the cell level between LLMs

and LAMs respectively. In addition data transfer and conversion can be performed between LAMs and LLMs.
Different analog VLSI implementations of CNN Universal Chips and a comparison of their performance characteristics can be found in Table 2 these chips were measured and tested in ANCL in Budapest. The first fully operational CNN-UM implementation that can run analogic algorithms is the 1995 mixed-signal version (it has an optical input) from Seville (a Revised Version of the 1994 prototype that was only partially functional). This chip, embedded into the CNN Prototyping System (CCPS), was used in various experiments validating some of the templates and algorithms developed earlier. The most promising is certainly the latest version of these implementations (Seville, 1998). It has a 64x64 CNN [30] array and in addition to the features shown in Table 2 allows the use of fixed-state map techniques, global logical lines and ARAMs during the algorithm synthesis. It is expected that this chip will be a good candidate in some industrial applications.

Place of design	**Berkeley & Munich**	**Seville**	**Seville**	**Berkeley**	**Helsinki**	**Seville**
Date of design	1993	1994	1995	1996	1997	1998
Array size	12x12	32x32	20x22	16x16	48x48	64x64
Cell type	DTCNN	Full-range	Full-range	Chua-Yang	Chua-Yang	Full-range
Technology	2µ	1µ	0.8µ	1µ	0.5µ	0.5µ
Time constant (τ)	300ns	-	400ns	27ns	50ns	250ns
Input	analog	binary & optical	binary & optical	Analog	Binary	Analog
Output	binary	binary	binary	Analog & binary	Binary	Analog & binary
APR	external	8	8	External	1	32
LLU	AND	program-able	program-able	Program-able	Program-able	Program-able
LLM	2	4	4	2	2	4
LAM	-	-	-	-	-	4

Table 2. Comparison of the performance characteristics of different CNN Universal Chips.

The optical implementations are in the state of research. An optical breadboard model built on a joint transform correlator (JTC) is used as an experimental setup. Simulation software packages are written and used to test the computational (optical feed-forward operations) and the basic optical features. Principles and architectures have been worked out to implement both B and A templates, but these are to be tested in the near future.

4 Programmable Opto-electronic Analogic CNN Computers (POAC)

The demand for fast identification and tracking of targets e.g. in surveillance systems has been increased dramatically during the last few years [31], [32]. In several other image-processing tasks the quick recognition of particular structures is also important.
The very fast, online pre- and post-processing of the flow of image data is inescapable. Optical information processing systems can provide appropriate speed to solve these demands. However, the so far published optical processing system architectures do not seem to be flexible enough to be applicable in different computational tasks.
In recent years, several studies have demonstrated that a cellular neural/nonlinear network (CNN) type architecture, provides exhaustive programming frame for several complex, image-processing tasks [33], [34]. While several emulated digital and mixed-signal analog

implementations are emerging, there have been only a few attempts to build optical or opto-electronic implementation [35]-[43] of the CNN-UM. Optical correlators, however, can implement one of the basic operations of CNN computation: the convolution.

New optical computer architecture is arisen [6]. Programmable Opto-electronic Analogic CNN Computers (POAC) combines programmability and optical computing, embedding CNN Universal Chips and optical holographic memories. This includes the integration of an optical processing system, usually an optical correlator, with the fast spatio-temporal processing capabilities of a CNN-UM chip for target detection. This approach seems to be useful from two points of view: It can combine the CNN-UM basically local processing – non-local, even wave based processing is solved by local feedback operations – with the optical system basically global operations. Otherwise, the CNN paradigm can provide a simple and universal algorithmic framework, which can be used also efficiently in programming of the optical processors.

4.1 Optical correlators

The joint transform correlator (JTC) [44], [45] is a powerful optical information-processing unit for pattern identification. It shows increased robustness comparing to a matched filter VanderLugt correlator (VLC). [46]

Advantages of JTC realization [47]-[54]:

- *Use of a spatial-domain (impulse response) filtering (no previous calculations and computer processing is needed to synthesize the Fourier–domain filters which are necessary for VLC).*
- *The JTC has a higher space-bandwidth product and a lower carrier frequency.*
- *It has a higher index modulation.*
- *It is suitable for real time applications.*
- *It is much more robust against vibrations and misalignment compared with the VLC and its robustness is comparable with that of the incoherent correlators.*

Drawbacks of JTC:

- *It suffers from moderate (lower) detection efficiency when applied to multiple target recognition or targets embedded in intense background noise.*
- *Furthermore, high spatial coherence is required, but it does not need large coherence length.*
- *The JTC method is less efficient from energetic point of view as the first order diffractive beam, which is providing the desired convolution, carries only about 1/8th of the incident energy.*

However, these drawbacks can be alleviated by applying recently developed methods (phase encoding - both in the spatial and Fourier domain -, zero-order elimination, incoherent hologram superposition and read-out)

The following equations (1,2,3) describe mathematically the operations of JTC.

$$Input = s(x + x_0, y) + t(x - x_0, y) \tag{2}$$

Where s and t corresponds to the input image and to the template.

$$\begin{aligned} &Joint\ Power\ Spectrum = S^2(\alpha,\beta) + T^2(\alpha,\beta) + \\ &+ S(\alpha,\beta)e^{-i\varphi_S(\alpha,\beta)} T(\alpha,\beta)e^{i\varphi_t(\alpha,\beta)} e^{-i2x_0\alpha} + \\ &+ S(\alpha,\beta)e^{i\varphi_s(\alpha,\beta)} T(\alpha,\beta)e^{-i\varphi_t(\alpha,\beta)} e^{i2x_0\alpha} \\ &where\ S(\alpha,\beta)e^{i\varphi_s(\alpha,\beta)}\ and\ T(\alpha,\beta)e^{i\varphi_t(\alpha,\beta)} \\ &corresponds\ to\ the\ Fourier\ transforms\ of \\ &s(x,y)\ and\ t(x,y). \end{aligned} \tag{3}$$

$$Output = s(x,y) * \bar{s}(x,y) + t(x,y) * \bar{t}(x,y) + \\ + \bar{s}(x - 2x_0, y) * t(x,y) + s(x + 2x_0, y) * \bar{t}(x,y) \quad (4)$$

The previous optical CNN implementations, however, had used mainly the VLC type correlator [36]. The main problem with optical CNN VLC implementation is the slow, offline construction of the appropriate complex, computer designed holographic filter, corresponding to the necessary template. This design is sensitive for the precise positioning of the elements.

4.2 Basic structure and function of this design

In our approach, the joint Fourier transform correlator (JTC) will be used in a novel way for preprocessing, since it accomplishes the basic feedforward-only CNN operations. For example, this makes it possible to realize e.g. mathematical morphology (MM) processing in the CNN framework. The basic plan of the JTC based POAC is shown in Figure 3.

In the proposed architecture the unknown input image from an electronically addressed spatial light modulator (ESLM) [55] or optically addressable spatial light modulator (OASLM) is correlated with the template(s) considered as reference image(s). Laser 1 is the coherent light source (red, He-Ne). Lens FL1 Fourier transforms the images on the OASLM in which the interference fringes are recorded.

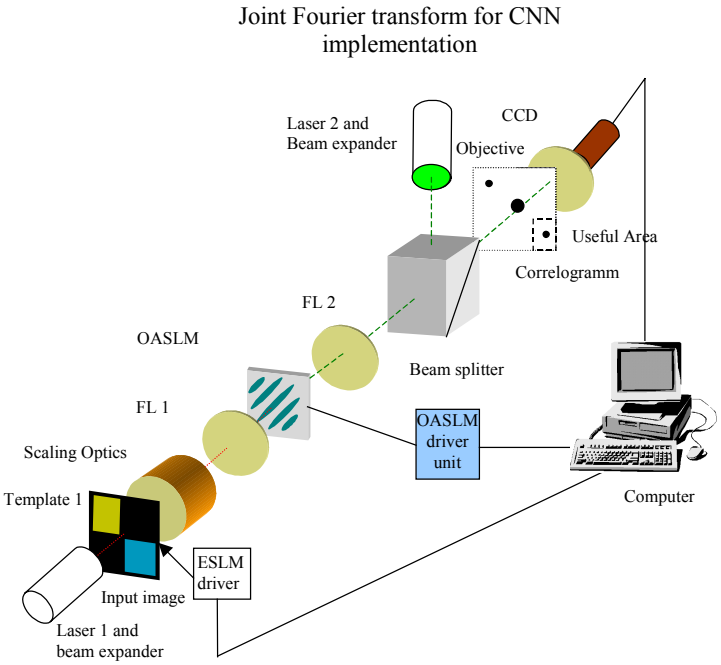

Figure 3. The experimental setup for JTC–CNN implementation measurements.

Presently, we use a moderate resolution OASLM from Jenoptik GmbH. To increase the processing capability, a higher resolution OASLM will be used. These high resolution OASLMs can be liquid crystal devices (e.g. from CoreTek Inc), PQW-SLMs (QuantaImage) or special bio-engineered materials like BR. The interferogram between the images is read-out by the light of laser 2 (green, He-Ne) and Fourier transformed by lens FL2 and projects the correlation peaks onto CCD camera. A personal computer (PC) is used to drive the image SLM.

So a classical JTC is installed with OASLM as the holographic material. Presently, both the input images and the templates are binary images. The output, the cross-correlation (convolution) terms, is recorded by a CCD camera. Next figure (**Figure 4**) shows the current optical correlator setup.

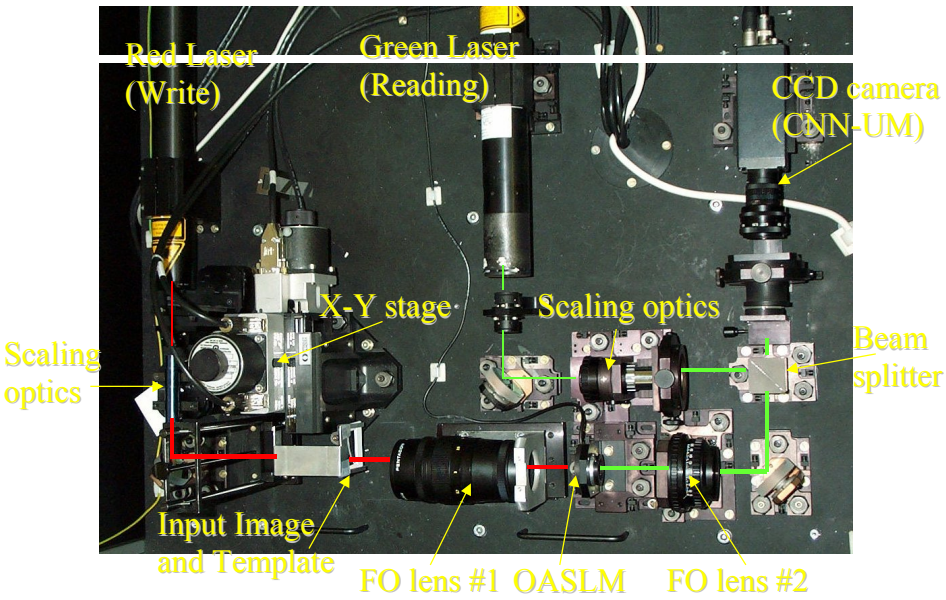

Figure 4. Current POAC JTC optical correlator setup

4.3 Improved JTC architecture

More complicated processing can be carried out by the composition of our optical CNN implementation with CNN-UM chips. The basic structure of the proposed architecture can be seen in Figure 5. Possible advantages of POAC realization:

- *The large neighborhood templates can find complex images on the input image.*
- *A VLSI implemented CNN-UM can perform the necessary further computations, considering the feedback and complex algorithms.*
- *The CNN-UM can solve the adaptive scaling and thresholding of the optical feedforward only CNN (JTC) input*

So the optical, feedforward only CNN implementation's output can be the optical input of the VLSI CNN-UM chip.

By the modification of the amplitude distribution of the reading light beam we can implement an additional template operation. The scheme of this operation is also denoted in Figure 5. This architecture provides the possibility to ensure adaptively the balance between input image and primary template's illumination. If the primary template is only a dot (Dirac delta), the reconstructed correlation image should be the same as the input. By adaptive changes of the input image's illumination we can achieve optimal reconstruction. Assurance of this balance is essential and usually unavoidable for any type of further processing. In the followings we can use an additional template (t2 in Figure 5) for programming the POAC system. In this case much higher speed computation can be achieved, which works with speed of light.

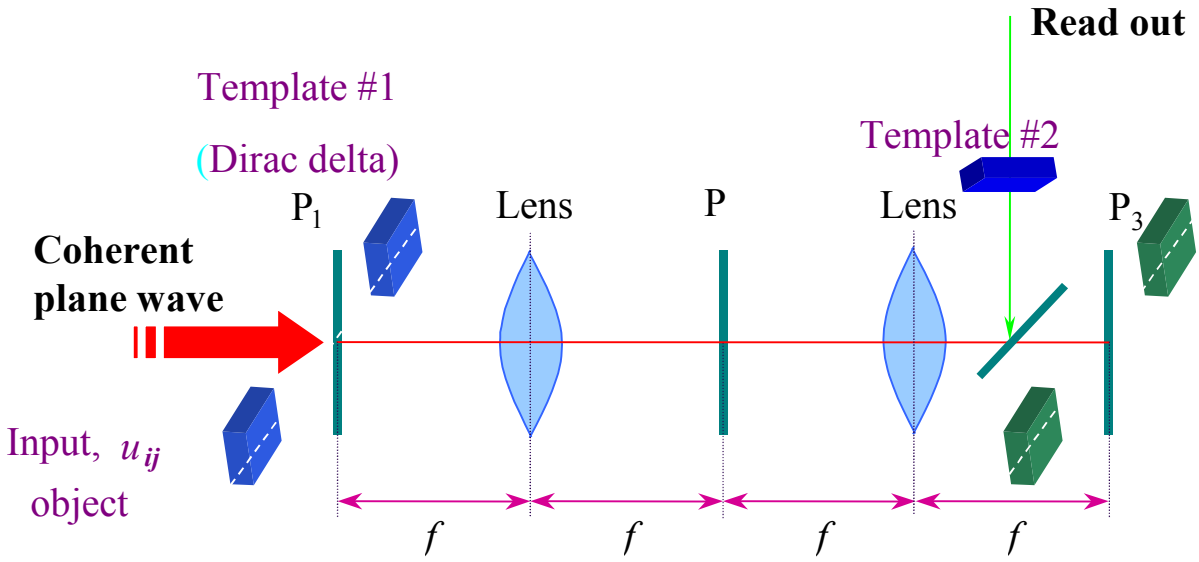

Figure 5. The proposed Programmable Opto-Electronic Analog CNN (POAC) computer architecture.

Mathematically the next equation can describe the operations.

$$\begin{aligned} Output &= F^{-1}((F(s(x-x_0)+F(t_1(x+x_0)))^2 F(t_2(x))) = \\ &= F^{-1}(T_2(\alpha)(F^2(\alpha)+T_1^2(\alpha)))+ \\ &+ \underline{\bar{s}(x-2x_0)*t_1(x)*t_2(x)}+ \\ &+ \underline{s(x+2x_0)*\bar{t}_1(x)*t_2(x)} \end{aligned} \qquad (5)$$

where F and F^{-1} are the Fourier transform and its inverse

4.4 Large neighborhood templates

Main advantage of the optical implementation, that there is no harsh limitation on the size of the applied templates as in the case of VLSI implementations. So by the POAC computer it is easy to implement multi-scale image processing tasks by applying a set of scaled templates.

4.5 Advantages

POAC has several advantages comparing the former approaches. It is combining high-speed analog optical and electronic processing with programmability. The CNN's nearest neighbor connectivity is extended by the optical system's much wider coupling. Within this architecture we can carry out computation in several levels of the processing, e.g. we can solve image processing tasks in the Fourier domain besides the image and correlation plane. By the CNN's optical implementation, arbitrary size of B template operation can be accomplished. Some of the processing can be executed at the speed of light. The bottleneck of the optical correlator and so the feedforward CNN optical implementation is the resolution of the OASLM. In the current setup we are using 30 line-pairs/mm resolution liquid crystal optically addressable spatial light modulator (Jen-optics). This fact presents severe limitations on the applicable optical devices (focal length and precision of the lens) and the possible size of the input images as well. Even the types of different feasible architectures are limited by this low resolution. The aimed decrease of the system size, prospective further miniaturization, also requires the application of a much higher resolution holographic material like BR.

5 BR in POAC

We intend to use BR as a transient holographic material within the POAC framework. Due to the BR high resolution and speed it can provides an excellent solution [54].

5.1 Dual axis JTC

In the current setup we are using joint transform correlator for the implementation of the convolution. However, in this architecture the employable surface of the input is relatively low so the majority of the applied light power is wasted. To increase the effective area of the input we should use a dual axis JTC architecture (see Figure 6). In this case the input image and the reference image (template) can utilize the whole surface of the ESLMs. Even an OASLM can be applied at the input. Dual axis JTC require high-resolution holographic material, therefore BR seems to be adequate for this purposes.

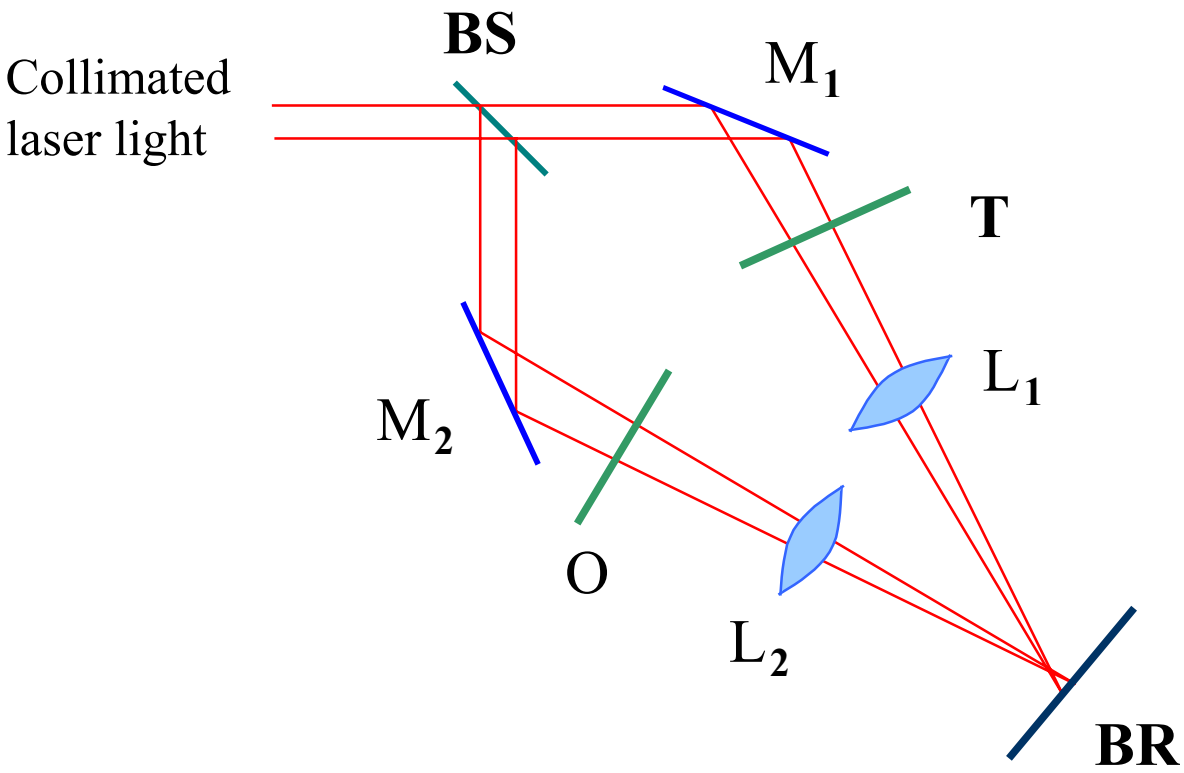

Figure 6. Dual axis architecture for holographic recording.

5.2 Possible Implementations

Due to the BR special structure, polarization holography (briefriengence) based architecture [56], [57], [58], [59], [60] seems to be fruitful for transient holographic recording. If the writing light beam is linearly polarized then only those molecules will absorb, whose orientation lies in the corresponding direction. Such a way photoinduced birefringence is achieved. This way BR can be write and read with the same wavelength, but of course with different intensity and polarization. This method simplifies the architecture and considerable noise removal is achievable. Next figure (Figure 7) depicts the architecture using BR with polarization holography for the POAC implementation. The writing wavelength has to be optimized for the efficiency of writing and also for the

necessary relatively big change of the refractive index. At this 'ideal' (635nm) wavelength, relatively chip and small diode lasers are available.

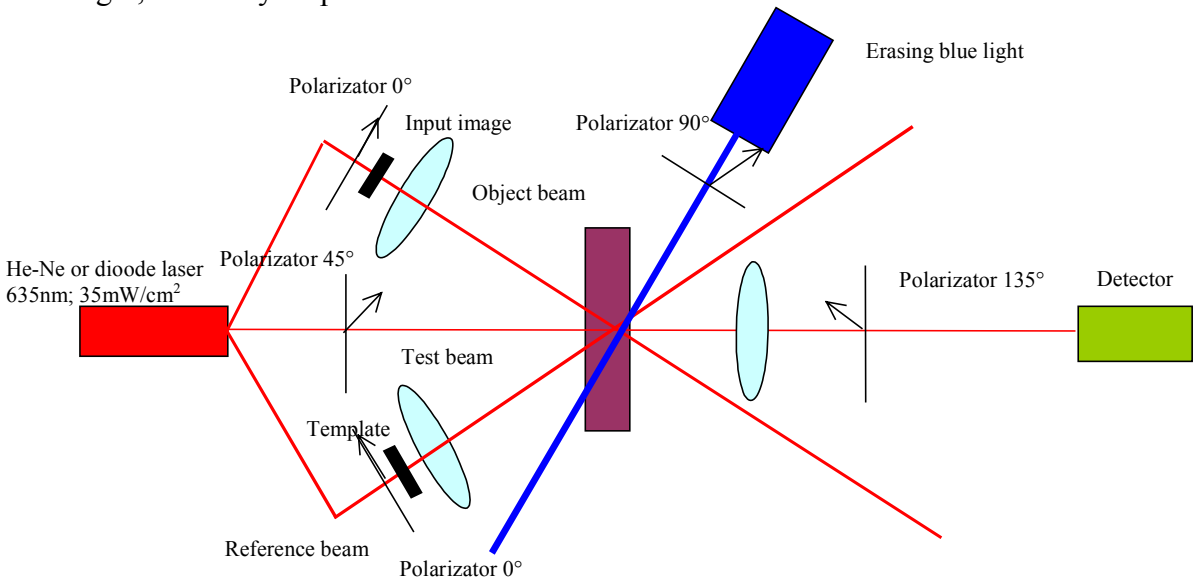

Figure 7. The bR birefringence is the strongest at the 635nm wavelength (20mW diode lasers can be achieved on this wavelength). The polarization of the object and reference beam is 45° to the perpendicularly oriented polarizator and analizator of the test beam, thus the bleached bR molecules can lead measurable modulation change. The applied blue light is polarized perpendicular to the object beams, so it can enhance the birefringence capacity of the material (drive the misleading M forms back to the BR state). Recorded holograms can be erased by a strong, blue light flashes. The cycle length can be decreased to 100μsec and so 10 kHz frame rate can be achieved. The actual architecture certainly different from the schematic one (writing and reading directions can be opposite etc.).

In our first experiments a more simplified BR JTC collerator architecture is suggested. In this case we use a single axis JTC setup and there would be only one Fourier optic lens in the system (Figure 8).

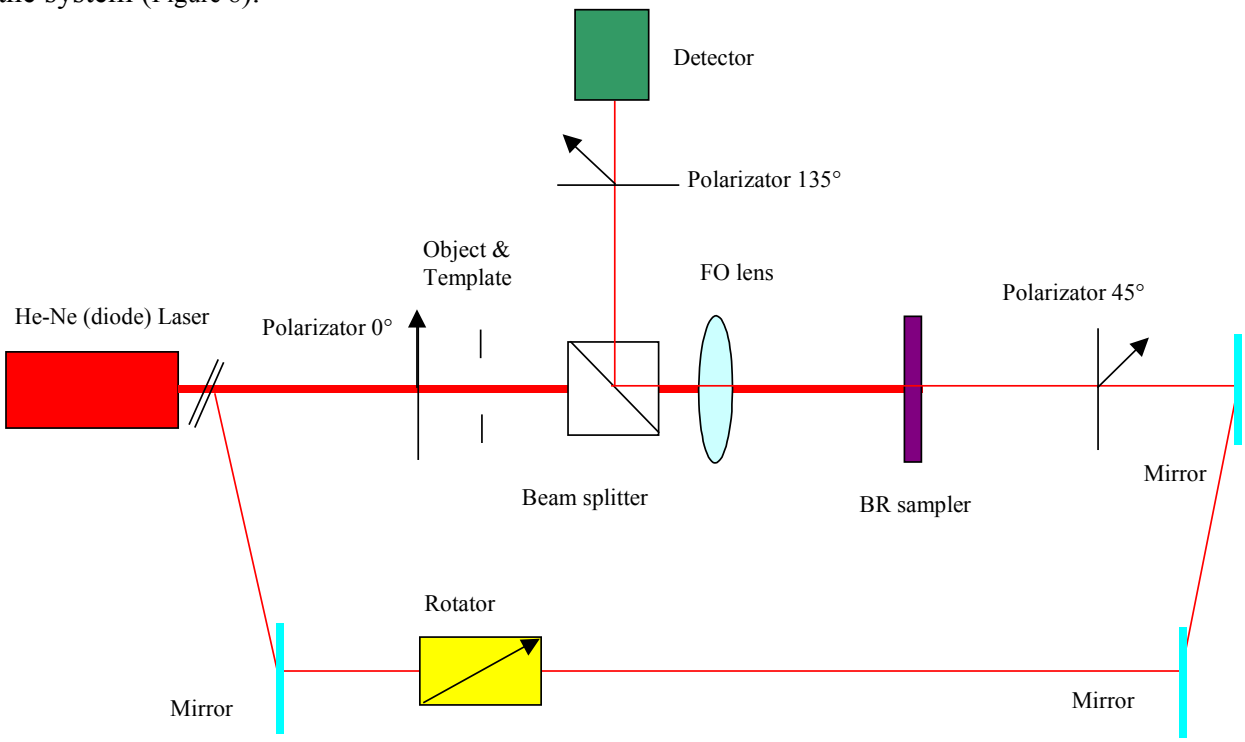

Figure 8. Simplified polarization holography based, single axis JTC BR correlator architecture.

There can be slight difference between the colors of the writing and reading lasers. In our original approach we used an architecture, where the writing (red) and reading (green) lasers were different. However the relatively thick BR films (high optical density is necessary for the desired big diffraction changes) can make this solution less feasible.

Refractive index changes can be utilized with or without the polarization holography. We can use these changes for phase modulation (same or different writing and reading wavelengths).

In our preliminary experiments we recognized that the classical JTC (even the dual axis JTC) architecture cause an inherent imbalance of the sample illumination. This highly unequal illumination causes the bleaching of the sample on some places besides the slowly responding places of the material. This uneven dynamics prevent the appropriate resolution holographic recording. To avoid these hindrances we used an alternative experimental setup: the fractional joint Fourier correlator architecture. That is, if we do not use lens the exact Fourier transform of the input image can be acquired in the infinite distance limit (see later). Alternatively we can implement this dual axis joint fractional Fourier correlator architecture using Fourier optic lens, but place the BR (or other type of holographic material) out of the exact focal plane (Figure 9).

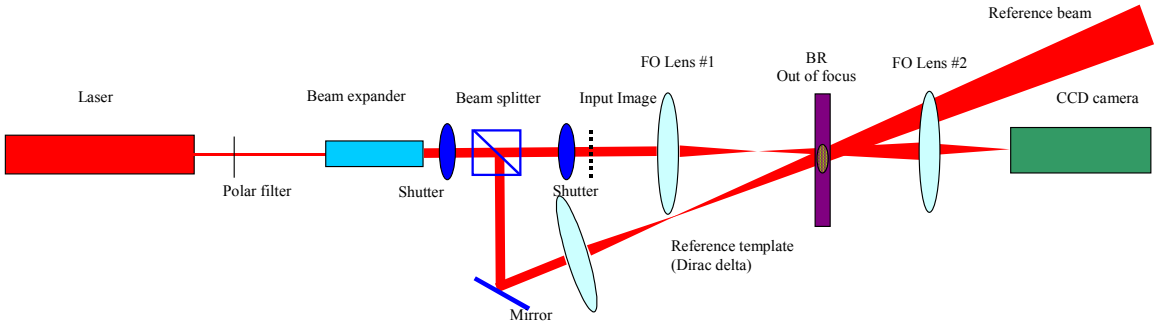

Figure 9. BR based dual axis joint fractional Fourier correlator implementation architecture. It works well. However, in a real optical CNN the reference (template) beams should cover the whole input image illuminated BR surface.

In these cases, however, we have to distribute the reference template beams over the image diffraction pattern. This can be fulfilled by appropriate technical tricks: by appropriate micro lens array or by an apt angle expansion technique.

In the final optical CNN implementation, we want to use a fractional dual axis joint Fourier implementation with the previously described polarization holographic architecture.

5.3 Other Possible Architectures

BR provides the possibility of the further speeding up of the processing. If we use other states of the photocycle even nanosecond computation time seems to be achievable. Only the device's size and the light speed delimit it.

Applying alternative architectures - (see earlier) - we can do several operations with a recorded hologram. In this case the pace of the template change and the applied detector's speed define primarily the overall performance.

6 Preliminary measurements

To test the applicability of BR as a holographic recording material in the POAC system, several measurements have been done.

We have examined, what is the achievable resolution with our BR samples. These samples were TEA modified, dry BR films with 20μm wideness [4].

It should be note, that the overall speed of the photocycle changes in different modified BR forms (AP, wild type, TEA, humidity, temperature etc.):
We measured the resolution of the BR samples by self-diffraction.

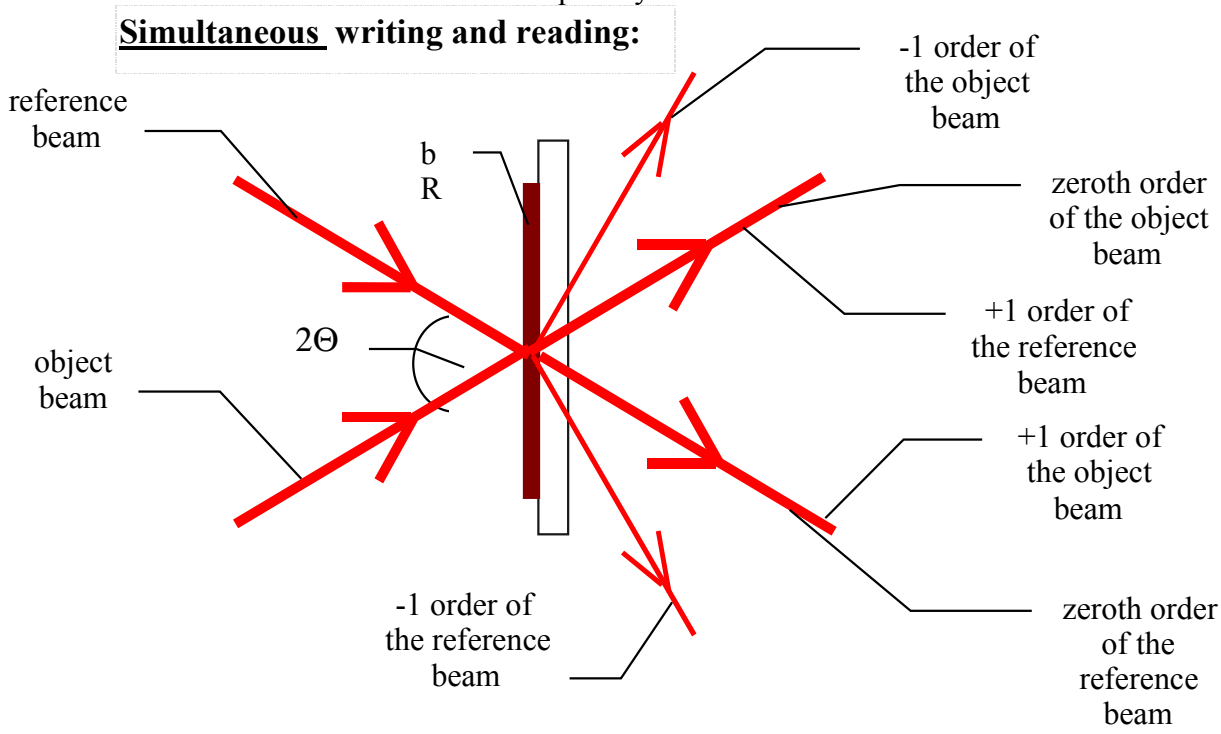

Figure 10. Self diffraction experiment

Initially the resolution appeared to be much lower (the maximal resolution was approximately 300 lines/mm (**Figure 11**)), than it is usually claimed in the BR literature (5000 lines/mm).

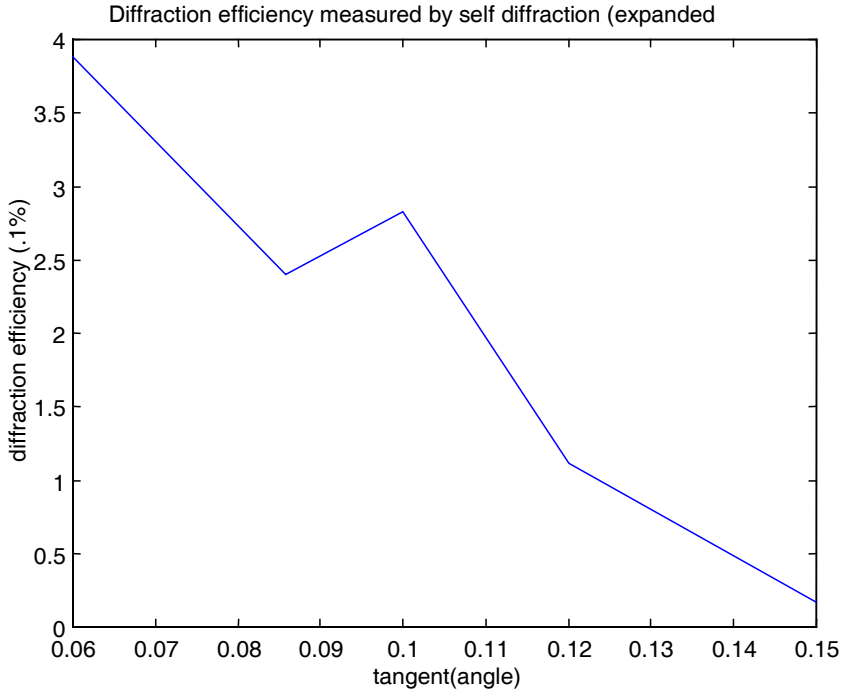

Figure 11. Self diffracted light (negative 1st order term) intensity as the function of the incident light intensity.

However, due to the fact that optical correlator architecture is to be implemented, the overall resolution is delimited by the resolutions of the lens and other optical elements

(300-400 lines/mm). So even this apparently ‘low’ resolution can be satisfactory for our purposes.
Originally we thought that although the resolution of the BR material is really high, the vibrations of the system degrade it. We tried to minimize and decrease the vibrations of our experimental setup, as it is always important in holographic recording. We used an optical bench (optical table with inner relaxation properties) with elastic basis (tennis balls). As we are not able to separate the noise sources, we have to use the system’s summed apparent resolution in our further design plans and experiments. In the expected optical CNN implementation architecture we have to consider a strict and rigid architecture to avoid vibrations. In our later experiments we determined that measured low and resolution dependent reduction of the diffraction efficiency was caused mainly not by the vibrations but the thickness of the medium (see later).

We could recognize remarkable dynamics in the BR sample’s response. That is, after an abrupt increase (the peak efficiency can be even higher than the measured one, but the used laser power meter device is relatively slow) the efficiency decreases considerably within fraction of seconds. It was caused the bleaching of the BR sample. Aggregating effects of vibrations can lead similar results. However, if we decreased the writing light intensity, the BR response is much slower and the effects of bleaching decreased. Oppositely, if we increased the writing light intensity the dynamics appears to be much faster and bleaching becomes more powerful.

Another finding of our experiments was that the positive and negative first order terms are not symmetric. There can be found relatively big amplitude (positive) first order terms under the zero order terms and it is more stable than the other (negative) first order term.

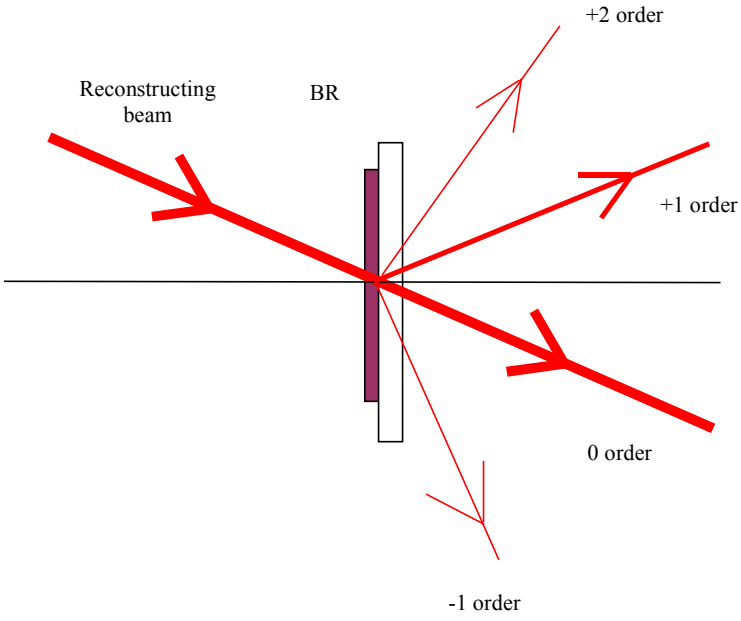

Figure 12. Asymmetry of the positive and negative terms in thick holographic recording in the BR sample.

We measured the diffraction efficiency of the positive first order term. We found that the diffraction efficiency was about 3‰ and it does not changed by the incident light beam angles (resolution) (as it was shown earlier [h]). It was still much higher than that of the (negative) first order term.

Our diffraction efficiency measurements were not too accurate – as it can be seen in the above figures - due to inherent dynamics of the material and the applied measuring method. Nevertheless it can corroborate, that the resolution of the BR is immense. More than 1000 lines/mm resolution is confirmed within our setup.

This detected asymmetry of the negative and positive first order terms is the consequence of the ‘thickness’ of the BR sample. As the resolution of the written gratings

increases the sample become relatively thick and in thick holograms only one of the first order terms are stable. Therefore, the measured low resolution was not the consequence of the vibrations but the thick holographic recording.

In the final architecture we have to consider the above outlined effects of the thick holographic recording in the BR samples. So it seems to be useful if the writing and reading light beams lies on the same axis or as close to each another as it can be.

We tested the BR samples holographic recording capabilities. We were able to store and recall relatively big (at least 200x200) gray-scale images. To demonstrate it, we show the raw data of our measurements.

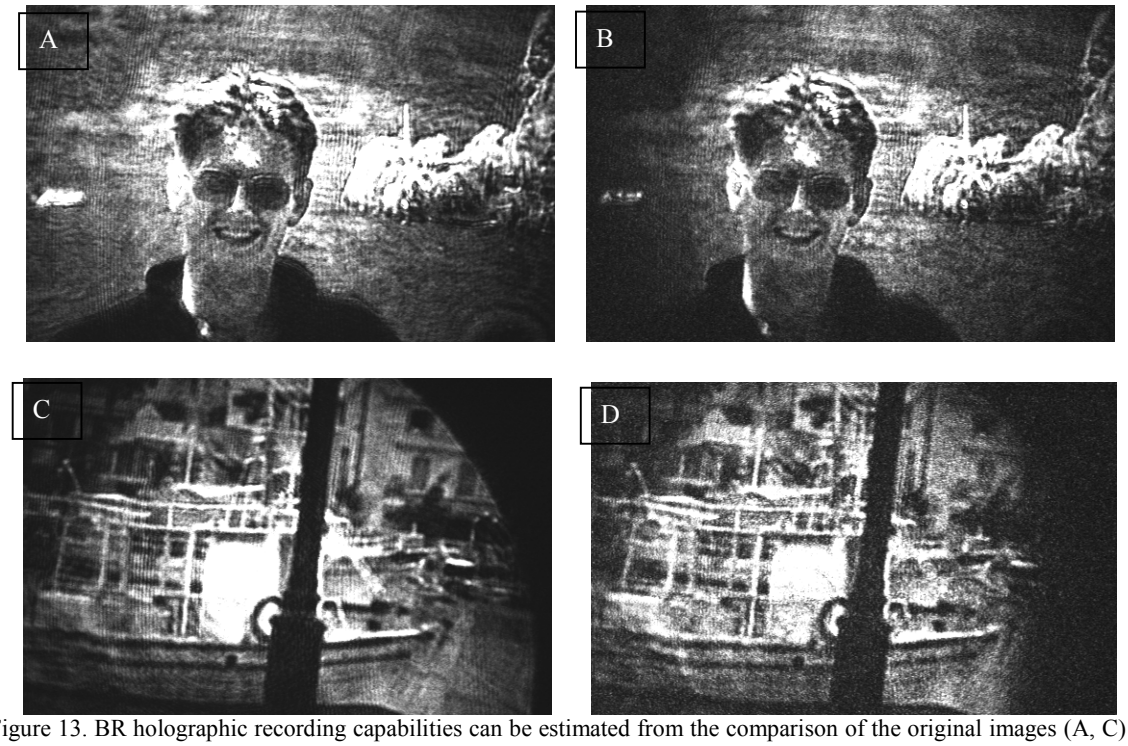

Figure 13. BR holographic recording capabilities can be estimated from the comparison of the original images (A, C) to the reconstructed images (B, D). The apparent coherent and other types of noises can be decreased in a more sophisticated setup. The input image (recording phase) illumination was decreased to avoid the saturation of the camera. But no consecutive image equalization, improvement has been done with the gained results.

Our results show that even the coherent and other types of noise were stored in the BR hologram. Reconstruction produced better performance than the optical system imaging capabilities.

7 Conclusion

We have been corroborated, as it was claimed earlier [61]-[66], that BR is an excellent choice for holographic recording material in POAC system. It can provide the necessary resolution and speed. We determined the preferred architecture to implement a BR based CNN implementation and a POAC system. Using molecular engineered versions or modified forms of this material and alternative architectures even the M-bR transition llimited (10KHz) speed can be accelerated. Applying this material in the POAC system immense reduction of the system's size is achievable also.

References

[1] D. Osterhelt, C. Brauche, N. Hampp, Bacteriorhodopsin: a biological material for information processing Quarterly Reviews of Biophysics, **24** (1991) 425-478.

[2] N.N. Vsevolodov, T.V. Dyukova, Retinal-protein complexes as optoelectronic components, Trends in Biotechnology **12** (1994) 81-88.

[3] Gy. Váró, L. Keszthelyi, Photoelectric signals from dried oriented purple membranes of halobacterium halobium. Biophys. J. Biophysical Society, **43** (1983) 47-51.
[4] M. Volperdinger, N. Hampp, Bacteriorhodopsin variants as versatile media in optical processing, Biophys. Chem. **56** (1995) 189-192.
[5] Z. Batori-Tartsi, K. Ludmann, Gy. Váró, The effect of chemical additives on bacteriorhodopsin photocycle,J. Photochem. Photobiol B. **49** (1999) 192-197.
[6] Sz.. Tõkés, L. Orzó, Cs. Rekeczky, Á. Zarándy, T. Roska, *An optical CNN implementation with stored programmability*, Proc. IEEE International Symposium on Circuits and Systems, May 2000, Geneva, pp. II-136 – II-139.
[7] L. O. Chua and L. Yang, Cellular Neural Networks: Theory, IEEE Trans. on Circuits and Systems, **35** (1988) 1257-1272.
[8] L. O. Chua and L. Yang, Cellular Neural Networks: Applications, IEEE Trans. on Circuits and Systems, **35** (1988) 1273-1290.
[9] L. O. Chua, and T. Roska, The CNN Paradigm, IEEE Trans. on Circuits and Systems, **40** (1993) 147-156.
[10] T. Roska and L. O. Chua, The CNN Universal Machine: an Analogic Array Computer, IEEE Trans. on Circuits and Systems, **40** (1993) 163-173.
[11] A. Dér, L. Oroszi, Á. Kulcsár, L. Zimányi, R. Tóth-Boconádi, L. Keszthelyi, Stoeckenius, W.; Ormos, P.: Interpretation of the spatial charge displacements in bacteriorhodopsin in terms of structural changes during the photocycle, Proc. Natl. Acad. Sci. USA, **96** (1999) 2776-2781.
[12] J.K. Lányi, Gy. Váró, The Photocycles of bacteriorhodopsin, Israel Journal of Chemistry, **35** (1995) 365-385.
[13] Gy. Váró, L. Keszthelyi, Arrhenius parameters of the bacteriorhodopsin photocycle in dried oriented samples, Biophys. J. Biophysical Society, **47** (1985) 243-246.
[14] T. Dyukova, B. Robertson, H. Weetall, Optical and electrical characterization of bacteriorhodopsin films, BioSystems **41** (1997) 91-98.
[15] Nikolai Vsevolodov, Biomolecular Electronics: An introduction via Photosensitive Proteins Birkhauser Boston, 1998
[16] R.R. Birge, M.B. Gillespie, E.W. Izaguirre, A. Kuznetzow, A.F. Lawrence, D. Singh, Q. Wang Song, E. Schmidt, J.A. Stuart, S. Seetharaman, K.J. Wise, Biomolecular Electronics: Protein-Based Associative Processors and Volumetric Memories J. Phys. Chem. B, **103** (1999) 10746-766.
[17] H. Imam, L.R. Lindvold, P.S. Ramanujam, Photoanisotropic incoherent-to-coherent converter using a bacteriorhodopsin thin film, Optics Letters, **20(2),** (1995)
[18] J. Joseph, F.J. Aranda, D.V. Rao, J.A. Akkara, M. Nakashima, Optical Fourier processing using photoinduced dichroism in a bacteriorhodopsin film, Optics Letters, **21(18),** (1996)
[19] T. Huang, K.H. Wagner, Photoanisotropic incoherent-to-coherent optical conversion, Applied Optics, **32(11),** (1993)
[20] J.D. Sánchez-de-la-Llave, M.A. Fiddy, Incoherent-to-coherent conversion and square-law transmission based on photoinduced birefringence in bacteriorhodopsin films, Applied Optics, **38(5)** (1999)
[21] T. Miyasaka, Design of Intelligent Optical Sensors with Organized Bacteriorhodopsin Films, Jpn. J. Appl. Phys. **34** (1995) 3920-3924.
[22] T. Okamoto, K. Yamagata, I. Yamaguchi, Real-Time Enhancement of Defects in Periodic Patterns Using Photoinduced Anisotropy of a Bacteriorhodopsin Film, Jpn. J. Appl. Phys. **36** (1997) L 1012- L 1014.
[23] A.L. Mikaelian, Holographic Memory and Some Applications, pp. 31-74 in Yu, F.T.S.; Yutamulia, S.(editors): Optical Storage and Retrieval, 1996.
[24] J.D. Sánchez-de-la-Llave, D.A. Pommet, Novel Joint transform correlator architecture using bacteriorhodopsin optically addressable spatial light modulators Optical Engineering, **37(1)** (1998) 27-32.
[25] G.I. Groma, G. Szabó, Gy. Váró, Direct measurement of picosecond charge separation in bacteriorhodopsin, Reprinted from Nature, **308(5959)** (1984) 557-558.
[26] G.I. Groma, F. Ráksi, G. Szabó, Gy. Váró, Picosecond and nanosecond components in bacteriorhodopsin light-induced electric response signal, Biophys. J. Biophysical Society, **54** (1988) 77-80.
[27] G.I. Groma, J. Hebling, C. Ludwig, J. Kuhl, Charge Displacement in Bacteriorhodopsin During the Forward and Reverse bR-K Phototransition, Biophysical Journal, **69** (1995) 2060-2065.
[28] K. Ludmann, C. Ganea, Gy. Váró, Back photoreaction from intermediate M of bacteriorhodopsin photocycle, J. Photochem. Photobiol. B: Biol. **49** (1999). 23-28.
[29] J.D. Downie and D.T. Smithey, Measurement of holographic properties of bacteriorhodopsin films" Appl. Opt. **35** (1996) 5780-5789.
[30] S. Espejo, R. Domínguez-Castro, G. Liñán, Á., Rodríguez-Vázquez, A 64×64 CNN Universal Chip with Analog and Digital I/O, in Proc. 5th Int. Conf. on Electronics, Circuits and Systems (ICECS'98), Lisbon, 1998, pp. 203-206.

[31] Javidi, J.L. Horner, Real-time optical information processing. Academic Press Inc. London, 1994
[32] F.T.S. Yu, S. Jutamulia, Optical pattern recognition. Cambridge University Press. 1998
[33] T. Roska, Computer-Sensors: Spatio-temporal Computers for Analog Array Signals, Dynamically Integrated with Sensors, Journal of VLSI Signal Processing Systems, **23(2/3)** (1999) 221-238.
[34] F. Werblin, T. Roska, and L. O. Chua, The Analogic CNN Universal Machine as a Bionic Eye, International Journal of Circuit Theory and Applications, **23**, (1995) 541-569.
[35] K. Slot, T. Roska and L.O. Chua, Optically realized feedforward-only Cellular Neural Networks, Memorandum UCB/ERL, Berkeley, University of California at Berkeley, 1991.
[36]. Frühauf, E. Lüder, M. Gaiada, and G. Bader, An optical implementation of space invariant Cellular Neural Networks, Proceedings of 10th European Conference on Circuit Theory and Design, (ECCTD'91), Copenhagen, 1991, pp. 42-51.
[37] Tien-Hsin Chao, Optical implementation of mathematical morphology in Optical Pattern Recognition, Editors F.T.S. Yu, S. Jutamulia, Cambridge University Press. 1998
[38] E. Lüder, N. Frühauf, Invited Lecture: Optical Signal Processing for CNNs, Proceedings of IEEE Int. Workshop on Cellular Neural Networks and Their Applications, (CNNA'92), Munich, 1992, pp. 45-54.
[39] K. Slot, Optically Realized Feedback Cellular Neural Networks, Proceedings of IEEE Int. Workshop on Cellular Neural Networks and Their Applications, (CNNA'92), Munich, 1992, pp. 175-180.
[40] K. Slot, T. Roska, L. O. Chua, Optically realized feedforward-only cellular neural networks, Archiv für Elektronik und Übertragungstechnik, (AEÜ), **46** (1992) 158-167.
[41] N. Fruehauf, E. Lueder, and G. Bader, Fourier Optical Realization of Cellular Neural Networks, IEEE Trans. on Circuits and Systems II: Analog and Digital Signal Processing, (CAS-II), **40(3)** (1993) 156-162.
[42] I. Andersson Stig, Recent Progress on Logic and Algorithms for Optical Neural Networks, Proceedings of IEEE Int. Workshop on Cellular Neural Networks and Their Applications, (CNNA'98), pp. 50-51, London, 1998
[43] S. Jankowski, R. Buczynski, A. Wielgus, W. Pleskacz, T. Szoplik, I. Veretennicoff and H. Thienpont, Digital CNN with Optical and Electronic Processing, Proceedings of 14 European Conference on Circuit Theory and Design, (ECCTD'99), Stresa, Italy, **2** (1999) 1183-1186.
[44] B. Javidi, J.L. Horner, Single SLM joint transform optical correlator, Appl. Opt. **28(5)** (1989) 1027-1032.
[45] K. Kodate, A. Hashimoto and R. Thapliya, Binary zone-plate array for a parallel joint transform correlator applied to face recognition, Appl. Opt. **38(14)** (1999) 3060-3067.
[46] VanderLugt, Signal detection by complex spatial filtering, IEEE Trans. Inf. Theory **IT-10** (1964) 139-145.
[47] F.T.S. Yu, Q.W. Song, Y.S. Cheng, D.A. Gregory, Comparison of detection efficiencies for VanderLugt and joint transform correlators, Appl. Opt. **29** (1990) 225-232
[48] F.T.S. Yu, E.C. Tam, T.W. Lu, E. Nishihara and T. Nishihara, Optical-disk-based joint transform correlator. Appl. Opt. **30** (1991) 915-916.
[49] P.S. Ramanujam, S. Hvilsted, R. Berg, Erasable holographic storage in novel azobenzene polyesters and peptides, SPIE Proceedings 3011 P32, (1997)
[50] F. Reichel, Properties and Application of Liquid Crystal Light Modulators in Optical Signal Processing Systems, OSA Tech. Digest Series **9** (1995) 32-35.
[51] R.C.D. Young, C.R. Chatwin, Experimental assessment of a photorefractive bandpass joint transform correlator Opt. Eng. **36(10)** (1997) 2754-2774.
[52] F.T.S. Yu, C.H. Zhang, Y. Jin and D.A. Gregory, Non-conventional joint transform correlator Opt. Lett. **14** (1989) 922-924.
[53] T.C. Lee, J. Rebholz and P. Tamura, Dual-axis joint-Fourier transform correlator. Opt. Lett. **4** (1979) 121-123.
[54] D. Osterhelt, C. Brauchle, N. Hampp, Bacteriorhodopsin: a biological material for information processing Quarterly Review of Biophysics. **24(4)** (1991) 425-478.
[55] T.D. Wilkinson, W.A. Crossland, V. Kapsalis, Binary phase-only 1/f joint transform correlator using a ferroelectric liquid-crystal spatial light modulator. Optical Engineering, **38(2)** (1999) 357-360.
[56] B. Borucki, H. Otto, M.P. Heyn, Linear Dichroism Measurements on Oriented Purple Membranes between Parallel Polarizers: Contribution of Linear Birefringence and Applications to Chromophore Isomerization, J. Phys. Chem. B **102**, 3821-3829 (1998)
[57] N.M. Burykin, E. Korchemskaya, M.S. Soskin, V.B. Taranenko, T.V. Dukova, N.N. Vsevolodov, Photoinduced anisotropy in bio-chrom films, Optics Communications, **54(2)** (1985)
[58] E.Y. Korchemskaya, M. S. Soskin, Polarization properties of four-wave interaction in dynamic recording material based on bacteriorhodopsin, Optical Engineering, **33(10)** (1994)
[59] E.Y. Korchemskaya, D.A. Stepanchikov, A.B. Druzhko, T.V. Dyukova, Mechanism of Nonlinear Photoinduced Anisotropy in Bacteriorhodopsin and its Derivatives, Journal of Biological Physic **24** (1999) 201-215.
[60] E.Y. Korchemskaya, D.A. Stepanchikov, T.V. Dyukova, Photoinduced anisotropy in chemically-modifed films of bacteriorhodopsin and its genetic mutants, Optical Materials **14** (2000) 185-191.

[61] A. Seitz, N. Hampp, Kinetic Optimization of Bacteriorhodopsin Films for Holographic Interferometry, J. Phys. Chem. B 2000, **104** (2000) 7183-7192.
[62] Q.W. Song, Ch. Zhang, R. Blumer, R.B. Gross, Zh. Chen, R.R. Birge, Chemically enhanced bacteriorhodopsin thin-film spatial light modulator. Optics Letters, **18(16)** (1993)
[63] Q.W. Song, Yu-He Zhang, Optical properties and applications of bacteriorhodopsin, in Yu, F. T. S.; Jutamulia, S.: Optical Pattern Recognition. Cambridge Univ. Press, 1998
[64] Yu-He Zhang, Q.W. Song, C. Tseronis, Real-time holographic imaging with a bacteriorhodopsin film, Optics Letters, **20(23)** (1995).
[65] N. Hampp, A. Popp, C. Brauchle, D. Oesterhelt, Diffraction efficiency of Bacteriorhodopsin films for holography containing bacteriorhodopsin wildtype BRwt and its variants BrD85E and BRD96N, J. Phys. Chem. **96** (1992) 4679-4685.
[66] R. Thoma, N. Hampp, Adaptive bacteriorhodopsin-based holographic correlator for speed measurement of randomly moving three-dimensional objects, Optics Letters **19(17)** (1994) 1364-66.